CHAPTER I

INTRODUCTION

Energy has great importance economically and plays a major role in the evolution of mankind worldwide. As such, it continuously and efficiently propels the world towards advancement. From ancient times till present, the trading of energy has become commercialized worldwide. Petroleum is the most eminent example, following by other forms of energy, such as coal, natural gases and electricity, which are harder to transport. The consumption of petroleum by cars' engines and manufacturing systems are from which our quality of life are improved. At the same time, petroleum plays the main role in terms of economics, politics and military of every country. Nevertheless, fossils fuel which is the main raw material to produce petroleum for the market is nonrenewable energy, thus we are trying to come out with other energy resources to reduce the demand of those nonrenewable energy such as biodiesel solar cell and gasohol.

1.1 Fuel cell

Fuel cells generate electricity from an electrochemical reaction in which oxygen (air) and a fuel (e.g. hydrogen) combine to form water. The electricity produced is used to power an electric traction motor in a vehicle. There are several different types of fuel cell but they are all based around a central design which consists of two electrodes, a negative anode and a positive cathode. These are separated by a solid or liquid electrolyte that carries electrically charged particles between the two electrodes. Several kinds of fuel cell are shown in Table 1.1.

Table 1.1 Types of fuel cells [1]

Fuel Cells name	Electrolyte	Operating Temperatures (°C)	Efficiency	Typical Electrical Power	Possible Applications
Alkaline Fuel Cells (AFC)	Potassium hydroxide	60-90 °C	45-60 %	Up to 20 kW	Submarines, spacecraft
Direct Methanol Fuel Cells (DMFC)	Polymer membrane	60-130 °C	45-60%	< 10 kW	Portable applications
Molten Carbonate Fuel Cells (MCFC)	Immobilised Liquid Molten Carbonate	650 °C	40%	> 1 MW	Power stations
Phosphoric Acid Fuel Cells (PAFC)	Immobilised Liquid Phosphoric Acid	200 °C	35-40%	>50 kW	Power stations
Proton Exchange Membrane Fuel Cells (PEMFC)	Ion Exchange Membrane	80 °C	40-60%	Up to 250 kW	Vechicles, small stationary
Solid Oxide Fuel Cells (SOFC)	Ceramic	1000 °C	50-65%	> 200 kW	Power stations

1.2 Solid oxide fuel cell [2]

Solid oxide fuel cells (SOFCs) have grown in recognition as a viable high temperature fuel cell technology. There is no liquid electrolyte with its attendant material corrosion and electrolyte management problems. The operating temperature of >800°C allows internal reforming, promotes rapid kinetics with nonprecious materials, and produces high quality byproduct heat for cogeneration or for use in a bottoming cycle. The high temperature of the SOFC, however, places stringent requirements on its materials. The development of suitable low cost materials and the low cost fabrication of ceramic structures are presently the key technical challenges facing SOFCs.

The solid state character of all SOFC components means that, in principle, there is no restriction on the cell configuration. Instead, it is possible to shape the cell according to criteria such as overcoming design or application issues. Cells are being developed in two different configurations, as shown in Figure 1-1. One of these approaches, the tubular cell, has undergone development at Siemens Westinghouse Corporation and its predecessor since the late 1950s. During recent years, Siemens Westinghouse developed the tubular concept to the status where it is now being demonstrated at user sites in a complete, operating fuel cell power unit of nominal 100 kW (net AC) capacities.
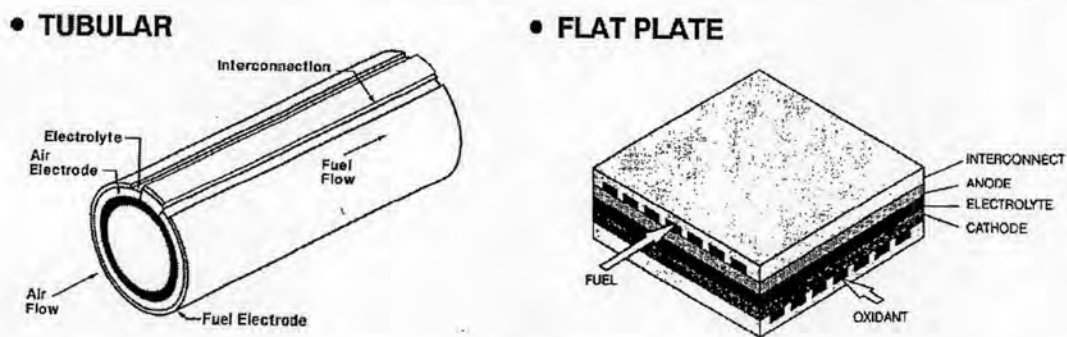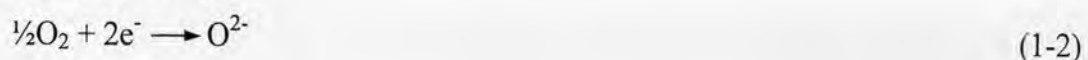

Figure 1.1 Solid Oxide Fuel Cell Designs at the Cathode [2].

The electrochemical reactions occurring in SOFC utilizing H_2 and O_2 are based on Equations (1-1) and (1-2):

$$H_2 + O^{2-} \longrightarrow H_2O + 2e^-$$
(1-1)

at the anode, and

$$\tfrac{1}{2}O_2 + 2e^- \longrightarrow O^{2-}$$
(1-2)

at the cathode. The overall cell reaction is

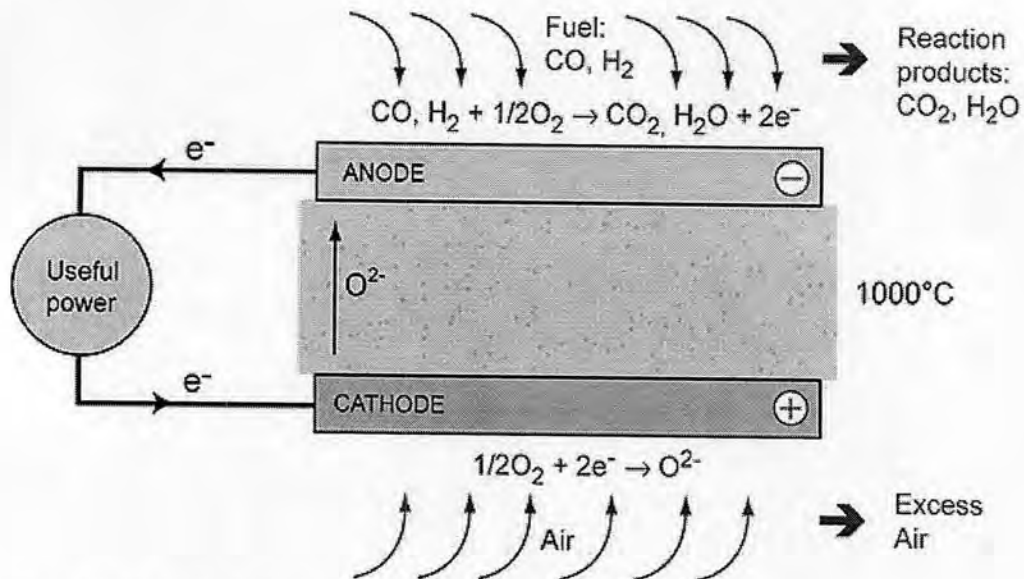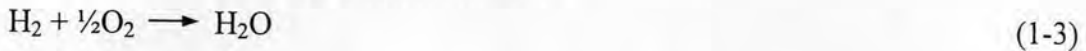$$H_2 + \frac{1}{2}O_2 \longrightarrow H_2O \qquad\qquad (1\text{-}3)$$

Figure 1.2 Solid Oxide Fuel Cell Operating Principle.

The operation of the solid oxide fuel cell is straightforward: oxygen atoms are reduced on the porous cathode surface by electrons. The oxide ions diffuse through the electrolyte to the fuel rich and porous anode, where they react with the fuel (hydrogen) and give off electrons to an external circuit. A large amount of heat is produced by the electrochemical reaction, which can be used by an integrated heat management system. Since it takes a long time to reach its operating temperature, the best applications for SOFCs are ones that uses both the heat and electricity generated: stationary power plants, auxiliary power supplies. Start-up time problems could be solved by using supercapacitor batteries for the first few minutes of operation in mobile applications.

1.2.1 Cathode [3]

The cathode operates in an oxidizing environment of air or oxygen at ~ 1000°C and participates in the oxygen reduction reaction, $1/2O_2 (g) + 2e^- = O^{2-}(s)$ i.e. oxygen in the gas phase is reduced to oxide ions, consuming two electrons in the process. The air electrode in solid oxide fuel cells has to meet the following requirements.

(a) High electronic conductivity.

(b) Chemical and dimensional stability in environments encountered during cell operation and during fabrication of interconnection, electrolyte and fuel electrode layers.

(c) Thermal expansion matchs with other cell components.

(d) Compatibility and minimum reactivity with the electrolyte and the interconnection with which air electrode comes into contact.

(e) Sufficient porosity to facilitate transport of molecular oxygen from the gas phase to the air electrode / electrolyte interface.

1.2.2 Electrolyte

The properties of the most common materials used as electrolytes in SOFCs. It must be:

(a) Dense and leak tight.

(b) Stable in reducing and oxidising environments.

(c) A good ionic conductor at operating temperatures.

(d) Non-electron conductor.

(e) Thin to reduce ionic resistance.

(f) Extended in area for maximum current capacity.

(g) Thermal shock resistant.

(h) Economically processable.

The materials used, are solid, ion-conducting ceramics. There are two main groups of such ion conductors: fluorite structured and perovskite structured, besides new materials such as hexagonal structured oxides. In an oxide ion conductor, current flows by the movement of oxide ions through the crystal lattice. This is a thermally activated process, where the ions hop from one lattice site to the other (from one potential valley to the other) in a random way. When an electric field is applied, there is a drift in one direction superimposed on the random thermal motion.

1.2.3 Anode

The fuel electrode must be stable in the reducing environment of the fuel, should be electronically conducting, and must have sufficient porosity to allow the

transport of the fuel to and the transport of the products of fuel oxidation away from the electrolyte / fuel electrode interface where the fuel oxidation reaction takes place, i.e.: $O^{2-}(s) + H_2(g) = H_2O(g) + 2e^-$.

1.2.4 Interconnection

Interconnection serves as the electric contact to the air electrode and also protects the air electrode material from the reducing environment of the fuel on the fuel electrode side. The requirements of the interconnection are the most severe of all cell components and include the following.

(a) Nearly 100% electronic conductivity.

(b) Stability in both oxidizing and reducing atmospheres at the cell operating temperature since it is exposed to air (or oxygen) on one side and fuel on the other.

(c) Low permeability for oxygen and hydrogen to minimize direct combination of oxidant and fuel during cell operation.

(d) A thermal expansion close to that of the air electrode and the electrolyte.

(e) Non-reactivity with the air electrode, electrolyte and the electric contact material

1.3 Perovskite [4]

Perovskites is a large family of crystalline ceramics that derive their name from a specific mineral known as perovskite. The parent material, perovskite, was first described in the 1830's by the geologist Gustav Rose, who named it after the famous Russian mineralogist Count Lev Aleksevich von Perovski. Perovskite is the most abundant mineral on earth and have been of continuing interest to geologists for the clues they hold to the planet's history. It is believed that the Earth's lower mantle is similar to the upper mantle, so the geological intrest lies here. The upper mantle is 80% $(Mg, Fe) SiO_3$ and the lower mantle is believed to be the same and another theory has it at 90-100% of this perovskite.

1.3.1 Structure of perovskite oxides [4]

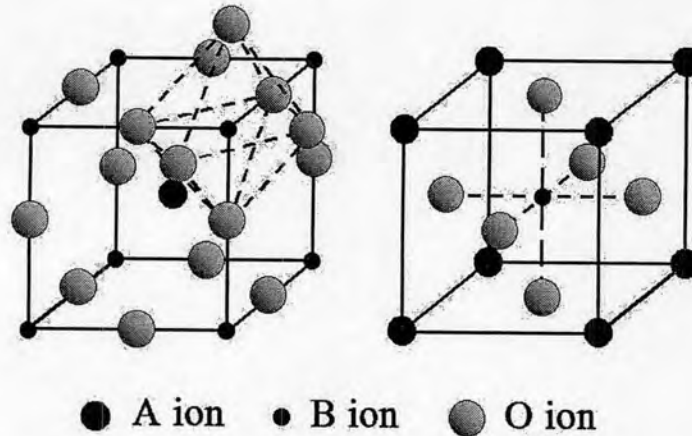### 1.3.1.1 ABO₃ - type

● A ion • B ion ⬤ O ion

Figure 1.3 ABO_3 ideal perovskite structure.

The principle perovskite structure found in ferroelectric materials is a simple cubic structure containing three different ions of the form ABO_3. A-site is Ln(lanthanides elements such as La), sometimes Ce, Pr, Ca, Sr, Ba). B-site is transition metals (Co, Mn, Fe, Cr, Cu, or V) or noble metals. In this structure, the B cation is 6-fold coordinated and the A cation is 12-fold coordinated with the oxygen anions.

In the ideal perovskite structure, the size and coordination preferences of three or more ions need to be satisfied simultaneously by the structure; it is, however, rarely possible that all these choice can be accommodated perfectly. This can be illustrated for the perovskite structure by deriving a relationship between the radii of the various ions. Figure 1.4 shows the relationship between ionic radii in the perovskite structure.
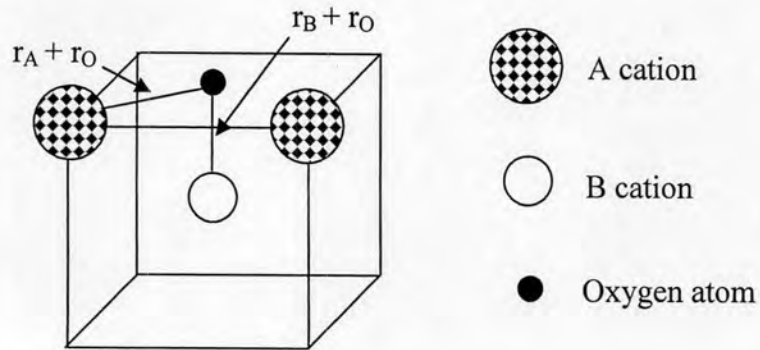
Figure 1.4 The relationship of ionic radii in perovskite structure.

$$a = 2xB - O = 2(r_B + r_O) \tag{1.4}$$

and

$$a = \frac{1}{\sqrt{2}} x 2 x A - O = \sqrt{2}(r_A + r_O) \tag{1.5}$$

hence,

$$2x(r_B + r_O) = \sqrt{2}x(r_A + r_O) \tag{1.6}$$

Where the atoms are touching one another, the B-O distance is equal to $a/2$ (a is the cubic unit cell parameter) while the A-O distance is ($a/\sqrt{2}$) and the following relationship between the ionic radius (r) holds shown in Equation 1.6. In general, the perovskite structure is formed if the tolerance factor, t.

$$t = \frac{(r_A + r_O)}{\sqrt{2}(r_B + r_O)} \tag{1.7}$$

The ideal perovskite is the cubic structure with the tolerance factor close to 1.0 at high temperature. The perovskite structure is stable in the range $0.75 < t < 1.0$, and is cubic in the range $t > 0.95$. Deviations from the ideal structure are well known as orthorhombic, rhombohedral, tetragonal, monoclinic and triclinic symmetry. The distorted structure may exist at room temperature but it transforms to the cubic structure at ambient temperature.

1.3.1.2 A_2BO_4 - type

A_2BO_4 oxides with the perovskite-related K_2NiF_4-type structure are less intensively investigated. This structure can be described as containing alternate layering of perovskite (ABO_3) and rock-salt (AO) units [5].
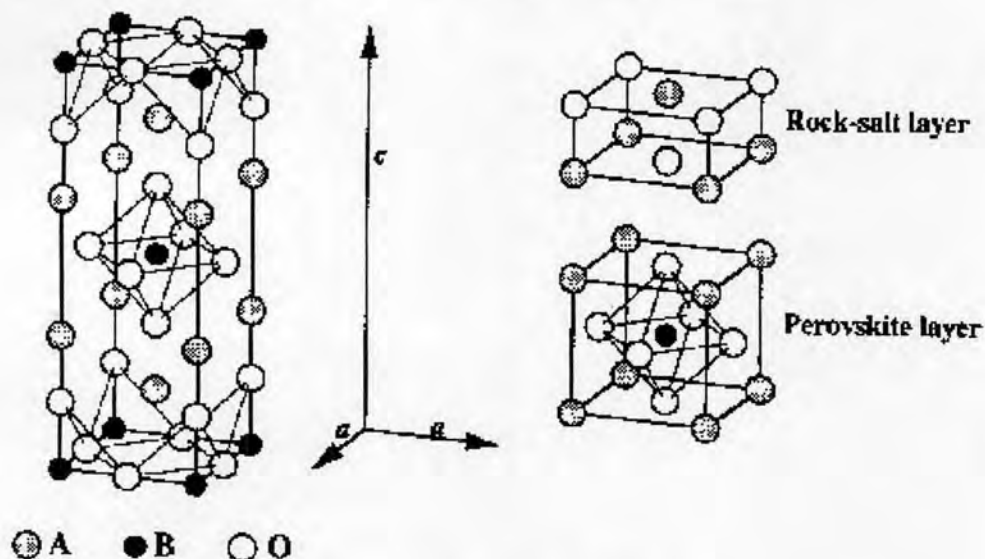

$\bigcirc A$ $\bullet B$ $\bigcirc O$

Figure 1.5 Crystal structure of A_2BO_4–type oxide.

Corresponding to the thermodynamic stabilities of the oxides within the range of phase stability, the oxide ABO_3 undergoes a partial reduction/oxidation reaction resulting in the well-known oxygen vacancy and electron hole-type defect structure, which determines the electrical transport properties of the oxides.

$$ABO_3 = ABO_{3-x} + x/2 \; O_2 \qquad\qquad (1.8)$$

At higher temperatures and lower oxygen partial pressures, the ABO_3 phase becomes unstable and reacts to A_2BO_4:

$$2 \; ABO_3 = A_2BO_4 + BO + 1/2 \; O_2 \qquad\qquad (1.9)$$
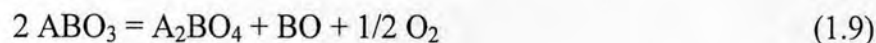
Reaction (1.9) can be assumed as a proof of the higher thermochemical stability of the A_2MO_4-type compounds compared with the AMO_3-type oxides. A_2MO_4-type oxides undergo partial reduction/oxidation reactions as well, corresponding to their thermodynamic stabilities within the range of existence of the phase.

$$A_2BO_4 = A_2BO_{4 \pm x} \pm x/2 \; O_2 \qquad\qquad (1.10)$$

The regular oxygen sites within the K_2NiF_4-type structure are completely occupied at an oxygen stoichiometry of 4.0. In compositions with $A+A'$ >1 excess oxygen ions may occupy interstitial oxygen sites as demonstrated by structure investigations.

1.3.2 Physical properties of perovskite

Perovskites with transition metal ions (TMI) on the B site show an enormous variety of intriguing electronic or magnetic properties. This variety is not only related to their chemical flexibility, but also and to a larger extent related to the complex character that transition metal ions play in certain coordinations with oxygen or halides. While magnetism and electronic correlations are usually related to unfilled 3d electron shells of the TMI, pronounced dielectric properties are connected with filled 3d electron shells. Multiferrocity, a coexistence of spontaneous ferroelectric and ferromagnetic moments, is a rare phenomenon due to the small number of low-symmetry magnetic point groups that allow a spontaneous polarization.

1.3.2.1 Dielectric and ferroelectric perovskites

High dielectric permittivity (ε) or ferroelectric materials are of enormous importance as electroceramics for engineering and electronics. Perovskites, *e.g.* titanium or niobium perovskites, $BaTiO_3$ and $LiNbO_3$, have been intensively studied in the past. A large ε is based on collective polar displacements of the metal ions with respect to the oxygen sublattice and is a highly nonlinear and anisotropic phenomenon. Relaxor ferroelectrics show enormously large dielectric constants, a pronounced frequency dispersion and variation of ε as function of temperature. These effects are due to slow relaxation processes for temperatures above a glass transition. The length scales of fluctuating composition and spontaneous polarization are 2-5 nm, i.e. the effects are based on electronic inhomogeneities and the existence of polar nanoregions. The lattice part of the response is considered to be a local softening of transverse-optical phonon branch that prevents the propagation of long-wavelength ($q = 0$) phonons. It is interesting to note that the fundamental limit, the superparaelectric state, is still not reached for such small

length scales. Incipient ferroelectrics or quantum paraelectrics can be regarded as almost ferroelectric crystals. Examples are $KTaO_3$ and $SrTiO_3$. Pronounced quantum fluctuations of ions suppress the phase-transition into the ferroelectric state and stabilize the soft transverse optical mode. The dielectric susceptibility shows a divergence in the limit T to 0 K together with pronounced phonon anharmonicities. In these systems even minor substitutions or doping can induce phase transitions into ferroelectric states. Finally, it can mentioned that perovskites related oxides with giant dielectric constants (GDC) where no evidence for a ferroelectric instability exists. These nonintrinsic permittivities are attributed to barrier layers and surface effects. Examples are $CaCu_3Ti_4O_{12}$, and the Li-ion conductor material $La_{0.67}Li_{0.25}Ti_{0.75}Al_{0.25}O_3$.

1.3.2.2 Magnetism and electronic correlations

In the ideal cubic perovskites structure, each oxygen is shared by two B^{3+} ions, forming a B-O-B angle of 180°. Such a configuration is favorable for superexchange interactions between magnetic B^{3+} cations. This exchange usually results in antiparallel coupling of nearest-neighbor magnetic moments. When the B^{3+} ions are in two sublattices ($A_2BB'O_6$) other spin arrangements are possible. If B' is a diamagnetic ion, the B^{3+} ions are aligned antiferromagnetically, and the most important exchange mechanism is believed to be a longer range superexchange interaction through two oxygens of the type B-O-B'-O-B. The B-B separation is now considerably longer than the 0.4 nm separation found in the ideal perovskite. The $LnFeO_3$ (Ln, lanthanide) perovskites are those that have attracted the most attention because of their possible applications as technological magnetic materials. These compounds show a weak spontaneous magnetic moment, which is attributed to a slight canting of the iron moments, which are otherwise antiferromagnetically aligned. The iron moments align in such a way that the direction of easy magnetization is along the *a* or *c* axis of the orthorhombic cell. The weak ferromagnetic moment of 0.03-0.07 μ_B/mol lead to the materials being considered for memory devices. Similarly, $LnMnO_3$ shows very interesting magnetic properties. These manganites containing mostly Mn^{3+} or Mn^{4+} ions show antiferromagnetic behavior. However, ferromagnetic behavior is observed in the range from 25 to 35% Mn^{4+}. A weak magnetic interaction was found between Mn^{3+} ions, together with a negative interaction between Mn^{4+} ions and a strong positive

interaction between Mn^{3+} and Mn^{4+}. A similar kind of behavior was found for the combination of Co^{3+} and Co^{4+}, but the Cr and Fe compounds were found to be antiferromagnetic.

The electrical conductivity of perovskites also shows wide variations. Several compounds have been used for their dielectric properties, while others show metallic conductivity, although most are semiconductors. As for other compounds, the electrical behavior in perovskites depends on the outermost electrons, which may be localized at specific atomic sites or may be collective. Since localized electrons may carry a spontaneous moment, there is a strong correlation between the electrical and magnetic properties of perovskites. Rare-earth perovskites containing transition ions show widely differing electrical properties. The electrical properties of perovskites have aroused special interest since the discovery in 1986 of superconductivity at 40 K in cuprates These cuprates are hole superconductors, exhibiting a mixed valence of copper CuII-CuIII. Among these, the exception is Ce doped Nd_2CuO_4, with T_c close to 25 K, 34 which belongs to a different structural type and is an electron superconductor. All these compounds have a common feature, the bidimensional character of the structure, which has been shown to be an important factor for the existence of superconductivity at high temperature.

1.3.2.3 Mixed ionic-electronic conductors

Perovskites exhibits both ionic and electronic conductivity. When the B ions can take a mixed-valence state, charge neutrality is maintained by both the formations of oxygen vacancies and a change in the valence state of the B ions. The oxides may show both high oxygen ion conductivity due to the high oxygen vacancy concentration, and a high electronic conductivity due to the mixed-valence state [4]. The concentration of oxygen vacancies can also be increased by mild B-site ion substitution, such as Cu and Ni ions, which naturally take the divalent oxidation state [6]. If the valence state of the B ions is fixed, neutrality is maintained only by the formation of oxygen vacancies. The oxides may be predominantly ionic conductors, in this case.

1.3.3 Oxygen adsorption property

Oxygen adsorption on perovskite oxides has been studied mainly because of these compounds as redox catalysts. They were used for redox reactions in connection with purification of automobile exhaust gases [7]. Thus the study by temperature-programmed desorption (TPD) of oxygen adsorption on perovskite oxides has attracted considerable interest.

Yamazoe et al. [8] reported the first oxygen TPD results from perovskites. The objective was to study the influence of partial substitution of La^{3+} by Sr^{2+} in $La_{1-x}Sr_xCoO_3$ oxides on their surface and catalytic properties. Oxygen TPD peaks from perovskites appeared two oxygen desorption peaks after adsorption on $La_{1-x}Sr_xCoO_3$ at 1023 K. The low-temperature peak (α-type) was attributed to adsorbed oxygen, whereas the high- temperature peak (β-type) was ascribed to lattice oxygen. They concluded that the amount of desorbed oxygen from $La_{1-x}Sr_xCoO_3$ increased with increasing x-substitution. Since A-site substitution with a divalent ion is known to induce the formation of oxygen vacancies.

In a recent contribution, Yokoi and Uchida [9] observed that the amount of O_2 desorbed and the temperature of the α-type oxygen desorption from $LaMO_3$ (M = Cr, Mn, Fe, Co, Ni) tended to decreased with the increasing atomic number of the transition metal. The β-type oxygen desorption peak was found to be more specially associated with the M cation, although it is also affected by La-site substitution.

1.3.4 Nanotechnology [10]

The first use of the concepts in 'nano-technology' (but predating use of that name) was in "There's Plenty of Room at the Bottom," a talk given by physicist and chemist Richard Feynman at an American Physical Society meeting at Caltech on December 29, 1959. Feynman described a process by which the ability to manipulate individual atoms and molecules might be developed, using one set of precise tools to build and operate another proportionally smaller set, so on down to the needed scale. In the course of this, he noted, scaling issues would arise from the changing magnitude of various physical phenomena: gravity would become less important, surface tension and Van der Waals attraction would become more important, etc. This basic idea appears plausible, and exponential assembly enhances it with parallelism to

produce a useful quantity of end products. A number of physical phenomena become noticeably pronounced as the size of the system decreases. These include statistical mechanical effects, as well as quantum mechanical effects, for example the "quantum size effect" where the electronic properties of solids are altered with great reductions in particle size. This effect does not come into play by going from macro to micro dimensions. However, it becomes dominant when the nanometer size range is reached. Additionally, a number of physical (mechanical, electrical, optical, etc.) properties change when compared to macroscopic systems. One example is the increase in surface area to volume ratio altering mechanical, thermal and catalytic properties of materials. Novel *mechanical* properties of nanosystems are of interest in the nanomechanics research. The catalytic activity of nanomaterials also opens potential risks in their interaction with biomaterials.

1.3.4.1 Nanomaterials [11]

Nanomaterials are materials with morphological features smaller than a micrometre in at least one dimension. Despite the fact that there is no consensus upon the minimum or maximum size of nanomaterials, some authors restricting their size from 1 to 100 nm, a logical definition would situate the nanoscale between microscale (1 micrometre) and atomic/molecular scale (about 0.2 nanometers). See Figure "Classification of nanostructured materials".Materials reduced to the nanoscale can suddenly show very different properties compared to what they exhibit on a macroscale, enabling unique applications. For instance, opaque substances become transparent (copper); inert materials become catalysts (platinum); stable materials turn combustible (aluminum); solids turn into liquids at room temperature (gold); insulators become conductors (silicon). Materials such as gold, which is chemically inert at normal scales, can serve as a potent chemical catalyst at nanoscales. Much of the fascination with nanotechnology stems from these unique quantum and surface phenomena that matter exhibits at the nanoscale. Nanosize powder particles (a few nanometres in diameter, also called nanoparticles) are potentially important in ceramics, powder metallurgy, the achievement of uniform nanoporosity and similar applications. The strong tendency of small particles to form clumps ("agglomerates") is a serious technological

problem that impedes such applications. However, a few dispersants such as ammonium citrate (aqueous) and imidazoline or oleyl alcohol (nonaqueous) are promising additives for deagglomeration.

1.3.4.2 Nanoparticles

Nanoparticles or nanocrystals made of metals, semiconductors, or oxides are of interest for their mechanical, electrical, magnetic, optical, chemical and other properties. Nanoparticles have been used as quantum dots and as chemical catalysts. Nanoparticles are of great scientific interest as they are effectively a bridge between bulk materials and atomic or molecular structures. A bulk material should have constant physical properties regardless of its size, but at the nano-scale this is often not the case. Size-dependent properties are observed such as quantum confinement in semiconductor particles, surface plasmon resonance in some metal particles and superparamagnetism in magnetic materials.

Nanoparticles exhibit a number of special properties relative to bulk material. For example, the bending of bulk copper (wire, ribbon, etc.) occurs with movement of copper atoms/clusters at about the 50 nm scale. Copper nanoparticles smaller than 50 nm are considered super hard materials that do not exhibit the same malleability and ductility as bulk copper. The change in properties is not always desirable. Ferroelectric materials smaller than 10 nm can switch their magnetisation direction using room temperature thermal energy, thus making them useless for memory storage. Suspensions of nanoparticles are possible because the interaction of the particle surface with the solvent is strong enough to overcome differences in density, which usually result in a material either sinking or floating in a liquid. Nanoparticles often have unexpected visible properties because they are small enough to confine their electrons and produce quantum effects. For example gold nanoparticles appear deep red to black in solution.

Nanoparticles have a very high surface area to volume ratio. This provides a tremendous driving force for diffusion, especially at elevated temperatures. Sintering can take place at lower temperatures, over shorter time scales than for larger particles. This theoretically does not affect the density of the final product, though flow difficulties and the tendency of nanoparticles to agglomerate complicates

matters. The surface effects of nanoparticles also reduce the incipient melting temperature [10].
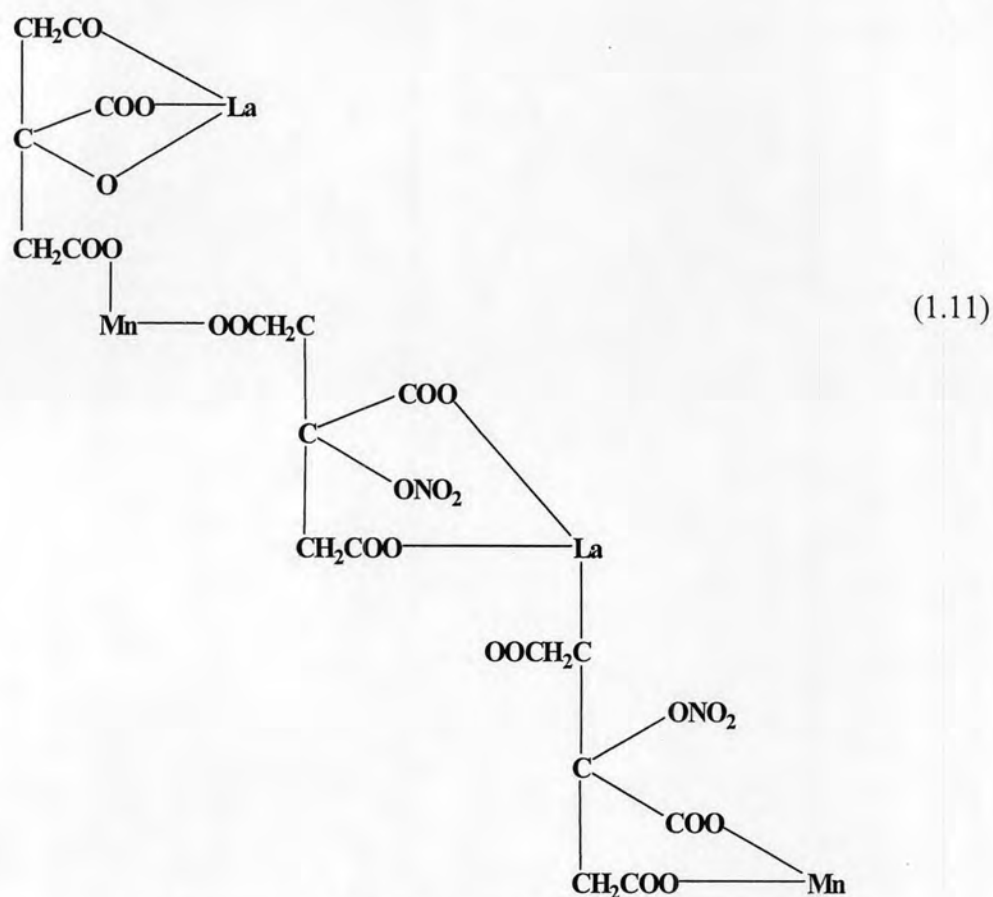
1.3.5 Perovskite synthesis

There are many routes to synthesize powders, such as a conventional solid-state reaction method and a wet chemical process that includes thermal decomposition of cyanide, metal–EDTA, chemical co-precipitation and the sol–gel process.

1.3.5.1 Solid-state reaction

The most common procedure for perovskite oxides synthesis via solid state reactions is the calcination of a homogenous mixture of the corresponding oxides and carbonates or nitrates. This method is very convenient but the impurities are introduced from raw materials, milling media, and the calcination container. Because of the high temperature required for the complete reaction. Problems such as multiphase have to be minimized in order to generate homogeneous high performance perovskite.
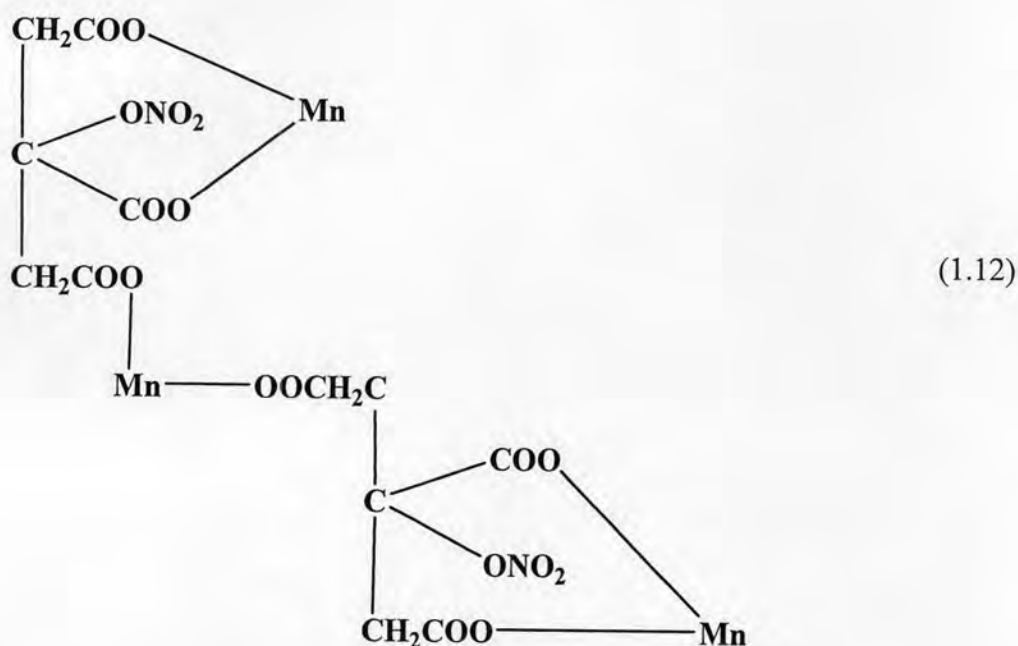
1.3.5.2 Sol-gel Process

The sol-gel process is a wet-chemical technique (Chemical Solution Deposition) for the fabrication of materials (typically a metal oxide) starting either from a chemical solution (sol short for solution) or colloidal particles (sol for nanoscale particle) to produce an integrated network (gel). Typical precursors are metal alkoxides and metal chlorides, which undergo hydrolysis and polycondensation reactions to form a colloid, a system composed of solid particles (size ranging from 1 nm to 1 μm) dispersed in a solvent. The sol evolves then towards the formation of an inorganic continuous network containing a liquid phase (gel). Formation of a metal oxide involves connecting the metal centers with oxo (M-O-M) or hydroxo (M-OH-M) bridges, therefore generating metal-oxo or metal-hydroxo polymers in solution. Sol-gel process involves producing precursor from citric acid and metal nitrate before thermal decomposition. For example Baythoun and Sale study the production of Sr-substituted $LaMnO_3$ perovskite powder by the amorphous citrate process. The manganese citrate-nitrate precursor may be represented as in Equation 1.11 [12]:

$$
\begin{array}{l}
\text{CH}_2\text{CO} \\
\quad\quad\text{COO} \longrightarrow \text{La} \\
\text{C} \\
\quad\quad\text{O} \\
\text{CH}_2\text{COO} \\
\quad\quad\text{Mn} \longrightarrow \text{OOCH}_2\text{C} \\
\quad\quad\quad\quad\quad \text{COO} \\
\quad\quad\quad\quad \text{C} \\
\quad\quad\quad\quad\quad \text{ONO}_2 \\
\quad\quad\quad\text{CH}_2\text{COO} \longrightarrow \text{La} \\
\quad\quad\quad\quad\quad\text{OOCH}_2\text{C} \\
\quad\quad\quad\quad\quad\quad\quad \text{ONO}_2 \\
\quad\quad\quad\quad\quad\quad \text{C} \\
\quad\quad\quad\quad\quad\quad\quad \text{COO} \\
\quad\quad\quad\quad\quad \text{CH}_2\text{COO} \longrightarrow \text{Mn}
\end{array}
\tag{1.11}
$$

In the complex the lanthanum is triply charged and replaces in one case the hydrogen of three –COOH groups (as in normal citrate formation) and in another case it replaces the hydrogen of one –OH group and two –COOH groups. Manganese in the divalent state replaces the hydrogen in two –COOH groups while NO_2 replaces the hydrogen of one –OH group.

In all cases the minimum amount of citric acid used was that necessary to bond the metals if all the NO_3^- ions were replaced. However, the amounts of metal and citric acid should not less than equimolar. If the high amount of citric acid was used, Mn_2O_3 was presented from the complex as in Equation 1.12:

CH₂COO, ONO₂, Mn, C, COO, CH₂COO

Mn — OOCH₂C, COO, C, ONO₂, CH₂COO — Mn

$$\begin{array}{l} \text{CH}_2\text{COO} \\ \qquad\quad \text{ONO}_2 \quad\quad \text{Mn} \\ \text{C} \\ \qquad\quad \text{COO} \\ \text{CH}_2\text{COO} \\ \\ \text{Mn}\!-\!\!-\!\text{OOCH}_2\text{C} \\ \qquad\qquad\qquad \text{COO} \\ \qquad\qquad\quad \text{C} \\ \qquad\qquad\qquad \text{ONO}_2 \\ \qquad\qquad \text{CH}_2\text{COO}\!-\!\!-\!\text{Mn} \end{array}$$

(1.12)

The formation of above structure would allow some citric acid, water, and nitrate ions to be lost during the preparation of gel. Every three molecules of citric originally present one remains uncombined and may be removed from the mixture by either evaporation or decomposition to yield acetone, carbon dioxide and water during the precursor preparation in the vacuum oven. The formation of this complex would also liberate NO_3^- groups for each two molecules of $Mn(NO_3)_2$ originally present in solution. The calcinations temperature should be higher than $800^{\circ}C$ because the wide range of homogeneity at lower temperatures was a result of the segregation of $Sr(NO_3)_2$ during precursor preparation and the production of $SrCO_3$ during precursor decomposition. However, it should not be higher than $1,100^{\circ}C$ because these would inevitably lead to a decrease in surface area. They also reported that the best compromise would appear and initial treatment of the precursor at $700^{\circ}C$ to yield the high surface area followed by an increase in temperature to $1,100^{\circ}C$ for a period of up to 4 hours to remove carbon.

The drying process serves to remove the liquid phase from the gel thus forming a porous material, then a thermal treatment (firing) may be performed in order to favor further polycondensation and enhance mechanical properties [13].

1.3.5.3 Hydrothermal synthesis

Hydrothermal synthesis can be defined as a method of synthesis of single crystals which depends on the solubility of minerals in hot water under high pressure. The crystal growth is performed in an apparatus consisting of a steel pressure vessel called autoclave, in which a nutrient is supplied along with water. A gradient of temperature is maintained at the opposite ends of the growth chamber so that the hotter end dissolves the nutrient and the cooler end causes seeds to take additional growth.

Possible advantages of the hydrothermal method over other types of crystal growth include the ability to create crystalline phases which are not stable at the melting point. Also, materials which have a high vapour pressure near their melting points can also be grown by the hydrothermal method. The method is also particularly suitable for the growth of large good-quality crystals while maintaining good control over their composition. Disadvantages of the method include the need of expensive autoclaves, good quality seeds of a fair size and the impossibility of observing the crystal as it grows [14].

1.3.6 Powder sizing

Powder particles are influenced on compacting and sintering. In most cases the objective of the pressing step is to achieve maximum particle packing and uniformity, so that minimum shrinkage and retained porosity will result during densification. A single particle size does not produce good packing. Optimum packing for particles all the same size results in over 30% void space. Adding particles of a size equivalent to the largest voids reduces the void pore volume to 23%. Therefore, to achieve maximum particle packing, a range of particle sizes is required.

Hard and dense agglomerates in ceramic powders usually result in large interagglomerate pores after sintering. Therefore small particle size is important because it facilitates the high strength of green disc and the sintering process. The primary driving force for densification of a compact powder at high temperature is the

change in surface free energy. Very small particles have high surface areas. The high surface free energy and very strong thermodynamic driving force decrease their surface by bonding them together. The particle with approximate sizes of 1 μm or less can be compacted into a porous shape and sintered at a high temperature to near-theoretical density [15]. Typically, the finer the powder, the greater its surface area, and the lower the temperature and shorter time for densification. Long time of the sintering temperature causes of the increasing in grain growth and lowering strength.

Calcined powder is not usually available with the optimum particle size distribution. The ball milling and screening are the common techniques to achieve the desire particle size of powder.

1.3.7 Powder compacting by uniaxial pressing

Uniaxial pressing is accomplished by placing the powder in to a rigid die and applying pressure along a single axial direction through a rigid plunger, or piston to achieve compacting. Pressing results in the direct contact of particles, reduces the average distance between particles, and changes the shape of particles. The apparent density of a compact was controlled by mixing of the proper various particles size fractions.

To enhance the compacting, before pressing, the powder should be disaggregated by mixing the powder with solvent such as isopropanol in the ultrasonic bath or added a couple drops of acetone to reduce the surface tension.

1.3.8 Sintering [16]

Sintering by definition is a process of permanent chemical and physical change accompanied by reduced porosity by the mechanism of grain growth and grain bonding. The driving force for sintering is the decrease in surface free energy that occurs as the surface area of the polycrystalline aggregate is reduced. This process can be achieved by solid-state reaction or alternatively in the presence of a liquid phase. When a powder aggregate is sintered, necks form between the particles, and the aggregate may increase in density. The growth of the neck is due to the transport of matter or of the counter-flow of vacancies between the particles and the pores. In crystalline powder, its transport occurs by diffusion

(bulk, surface, or grain boundary diffusion), whereas in amorphous materials, it occurs by viscous flow. Kuczynski has defined the neck growth as in Equation 1-13

$$X^n / r^m \quad = \quad kt \quad\quad\quad (1\text{-}13)$$

Where X and r are defined in Figure 2.3, t is the time, k is the temperature dependent constant, n and m are constants dependent on the mechanisms of growth, viscous or bulk diffusion, surface diffusion, or evaporation and condensation. Three stages of sintering can be distinguished. The early stage or initial stages during which the necks form at points of particle contact and the particles usually center approach each other. At this stage the individual particles are still distinguishable. The intermediate stage during that the necks become large, resulting in the formation of an interconnected pore structure. The third or the final stages during, the pores become isolated. Elimination of the interconnectivity of pores eliminates surface and vapor transport.

Closed pores isolated from grain boundaries shrink very slowly because grain boundary diffusion is far away from the pores. The growth of grains, therefore, hinders the attainment of theoretical density, since the pore's growth is also enhanced. It is essential, therefore, to retard grain growth so that densification of the compact can continue to the theoretical limit. This is particularly important with the present trend of using ultrafine particles as starting materials for the fabrication of technical ceramics. Surface diffusion becomes important in the case of very fine particles. Grain boundary diffusion and volume diffusion are the main mechanisms causing shrinkage of the neck, whereas surface diffusion does not contribute to any shrinkage. The most important diffusion paths during the sintering of two spheres with a grain boundary are surface diffusion, grain boundary diffusion, volume diffusion from the grain boundary to the neck surface, and volume diffusion from the sphere surface to the neck surface. The sintering rate also affected by the crystallization and growth processes, which occur concurrently. The sintering rate is reduced when there is intensive grain growth because when diffusion forms the pores occurs toward the boundaries of individual grains, the distance over which diffusion occurs with a reduction in pores is determined by the size of the crystals.
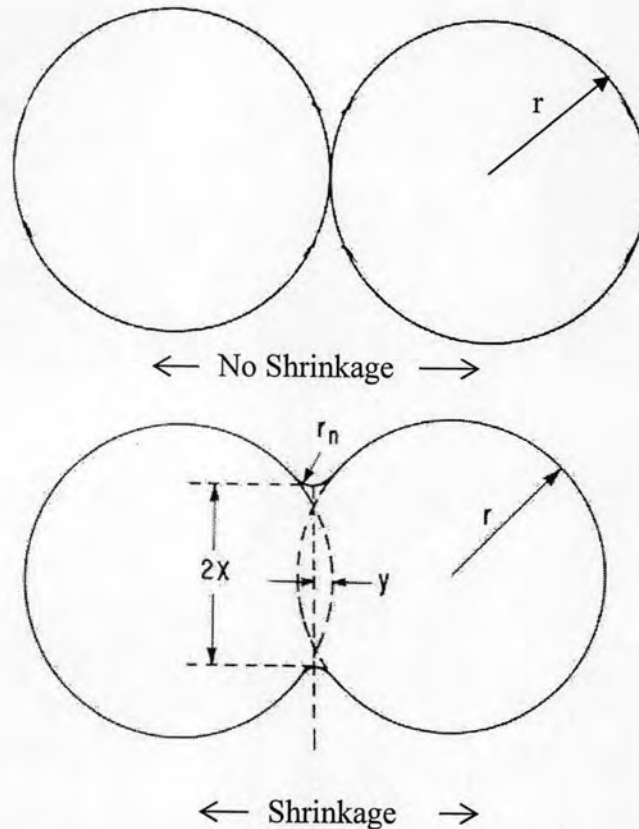
Figure 1.6 Mechanism of sintering; X is the internal radius of the neck; r is the particle radius.

1.4 Electrical measurement

1.4.1 Two-Point Measurements

$$R = \frac{V}{I} \tag{1-14}$$

Ohm's law is used in order to determine a resistance. A known current is sourced and flows through the unknown resistance. Measurement of the voltage develops across the resistance by dividing the measured voltage by the sourced current. A problem that occurs when using a 2-wire setup is that the voltage is measured not only across the resistance in question, but also includes the resistance of the electrode and contacts. When using an ohmmeter to measure resistances above a few ohms, this added resistance is usually 2-point measurement. However, when

measuring low resistances or when contact resistance may be high, obtaining accurate results with a two wire measurement could be a problem.
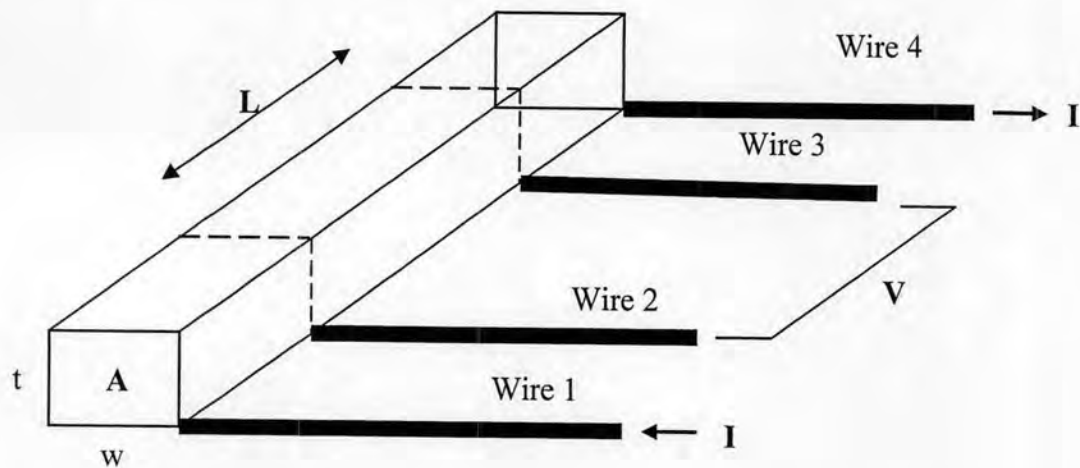
1.4.2 Four-Point Measurements

Figure 1.7 4-DC probe measurements.

A solution to the problem of 2-point measurements in which the lead and contact resistance is measured along with that of the device under test is the 4-wire or "Kelvin" measurement. Because a second set of probes is used for sensing and since negligible current flows in these probes, only the voltage drop across the device under test is measured. As a result, resistance measurement or I-V curve generation is more accurate.

The measurement method then includes a forced current I through the outer wires 1 and 4 and a measurement of the voltage drop over wire 2 and 3, using a very high Ohmic measurement device, so that the current flowing through wire 2 and 3 nearly zero. In that case the individual, additional contact resistance does not play a role as it cancels out of the equation. To study the behavior of the structure an I/V curve is generated, typically in the μA to the mA range. If the graph shows a straight line, the structure behaves as an Ohmic resistor. If assume that the resistance of a structure to be R then the following applies:

$$R = \frac{\rho L}{A} \qquad (1\text{-}15)$$

With   L = the length of the structure (m)

A = the area (width x thickness) of the cross section (m^2)

ρ = the specific resistivity (Ω.m of the practical unit $\mu\Omega$.cm)

1.5 Literature reviews

In 2000, Kharton, et al. [17] investigated effects of transition metal dopants on ionic conductivity of La(Sr)Ga(Mg,M)O $_{3-\delta}$ (M = Ti, Cr, Fe, Co, Ni). Oxygen-ion conductivity of the perovskite-type solid solutions $(La,Sr)Ga_{1-z}M_2O_{3-\delta}$ (M = Ti, Cr, Fe, Co; z = 0–0.20), $LaGa_{1-y-z}Mg_yM_zO_{3-\delta}$ (M = Cr, Fe, Co; y = 0.10–0.20, z = 0.35–0.60) and $LaGa_{1-z}Ni_zO_{3-\delta}$ (z = 0.20–0.50) was studied using the techniques of oxygen permeation, Faradaic efficiency, ion-blocking electrode and the e.m.f. of oxygen concentration cells. Oxygen-ion transference numbers vary from 2×10^{-6} to 0.98 throughout the series and p-type electronic conductivity increases with increasing transition metal content. Substitution of Ga with higher valence cations (Ti, Cr) decreases ionic conductivity whereas small amounts of Fe or Co (~5%) increase ionic conductivity. For higher transition metal contents, lower levels of oxygen-ion conductivity and an increase in the activation energy, E_A, for ionic transport, from 60 (5%-doped) to 230 kJ/mol (40%-doped) were observed. In heavily doped phases, E_A tends to decrease with temperature and, above 1170 K, values are similar to the undoped phase suggesting that an order–disorder transition had taken place.

In 2000, Yang, et al. [18] synthesized $SrCo_{0.8}Fe_{0.2}O_{3-\alpha}$ (SCFO) and $Ba_{0.5}Sr_{0.5}Co_{0.8}Fe_{0.2}O_{3-\delta}$ (BSCFO) using a combined citrate–EDTA complexing method. The results of O_2-TPD and XRD showed that the introduction of barium into SCFO could effectively suppress the oxidation of Co_3C and Fe_3C to higher valence states of Co_4C and Fe_4C in the lattice, and stabilize the perovskite structure under lower oxygen partial pressures. Oxygen permeation experiment showed that BSCFO membrane also had higher oxygen permeation flux than that of SCFO under air/He oxygen partial pressure gradient. At 950 °C, the permeation flux through 1.80 mm BSCFO membrane exposed to flowing predried air ($P'O_2$=0.21 atm) and helium ($P'O_{0.02}$=0.037 atm) is ca. 1.4 ml/cm^2 min and the activation energy for oxygen transportation is 40.9 kJ/mol within the temperature range of 775–950°C. The permeation flux of BSCFO was less sensitive to minor amounts of CO_2 and water vapor presented in the air than that of SCFO. Long-term oxygen permeation

study of more than 1000 h at 850°C indicated that the BSCFO membrane could operate stably as an oxygen generator at that temperature. A very slow exponential decay in the measured oxygen permeation flux occurred at temperatures lower than 825°C, which was caused by a phase transition. The phase transition was found to be reversible at higher temperatures, but a long time was needed for the equilibration.

In 2003, Shankar, et al. [19] reported a novel, low temperature (450–600°C) route for the synthesis of highly crystalline and homogeneous nanoparticles of lanthanum calcium manganese oxide $La_{0.67}Ca_{0.33}MnO_3$ (LCMO). The nanocrystallites, with average particle size of 30 nm, possess a ferromagnetic–paramagnetic transition temperature (T_c) of 300 K, which is about 50 K higher than that of a bulk single crystal. The transition temperature was found to be inversely proportional to the particle size. The Rietveld analysis of the powder X-ray diffraction data of the phase-pure nanopowders revealed that the particle size reduction leads to a significant contraction of the unit cell volume and a reduction of the unit cell anisotropy. Thus, it was proposed that these two lattice effects are responsible for the observed enhancement in T_c.

In 2005, Bos'kovic', et al. [20] determined a highly effective and simple procedure for synthesis of $CaMnO_3$, which are good candidates for SOFC components. Glycine nitrate process (GNP) was modified (MGNP) by partial substitution of nitrates for acetates. The combustion process proceeded very smoothly and single phase nanopowders with high specific surface (among highest published) area were obtained.

In 2006, Calder'on-Moreno, et al. [21] prepared $LaNiO_3$ nanopowder by an amorphous citrate route. It's an aqueous solution technique with simple and easy to use technological methods for preparing single-phase ceramic powders with controlled and homogeneous grain size. This study presents the preparation of ferroelectric $LaNiO_3$ ceramic samples by a gel-method using low sintering temperatures and the evolution of the amorphous complex and $LaNiO_3$ nanocrystallites with temperature. Ferroelectric $LaNiO_3$ powders were prepared using an 'amorphous citrate' route. X-ray diffraction, Raman scattering and electron microscopy techniques were used to characterize the obtained products after thermal treatments at between 550 and 750°C and revealed the formation of $LaNiO_3$ nanocrystallites of perovskite structure with homogeneous grain size after thermal treatment at 650, 700 and 750°C, with particle sizes of ~30, 42 and 65 nm, respectively. Raman spectra exhibit the characteristic band of the $LaNiO_3$ perovskite-phase at 392 cm^{-1}

and decreasing band width with temperature, an effect associated to the observed change in grain size.

In 2007, Ianculescu, et al. [22] investigated $Ba_{1-x}Sr_xTiO_3$ ($x = 0$, 0.20, 0.25, 0.30 and 0.35) nanopowders that prepared by Pechini method from titanium isopropoxide, barium and strontium carbonates using citric acid as a chelating agent and ethylene glycol as an esterification agent. X-ray diffraction data show the formation of $(Ba,Sr)TiO_3$ solid solutions, free from secondary phases as $BaCO_3$ or Ti-rich oxides, when the polymeric precursors were calcined in air at 850°C for 2 h. Ceramic pellets with relative density of 85–93% were obtained after sintering at 1350°C for 3 h. High values of the dielectric constants (of ~1,500–12,000), low losses at the room temperature and a shift of the ferro-para phase transition temperature in the range of 7–127°C with x decreasing were found. Lower values of the Curie constant for higher x indicate the increase of the chemical and electrical local heterogeneity degree.

In 2006, Ishihara, et al. [23] synthesized $La(Sr)Ga(Fe,Mg)O_3$, which exhibited the high oxide ion conductivity and investigated the electrical power generating property of SOFC single cell using $La_{0.7}Sr_{0.3}Ga_{0.7}Fe_{0.2}Mg_{0.1}O_{3-\delta}$ (LSGFM) electrolyte. The transport number of oxide ion is almost 0.8 in LSGFM and so open circuit potential (OCV) is as low as 0.8 V. OCV was strongly affected by anode materials and the highest OCV was achieved on Ni–Fe bimetallic anode. The extremely high power density was achieved by using LSGFM for electrolyte of SOFC. The maximum power densities of the cells can be elevated by coating with oxide ion conductor film at anode side. The maximum power density increased in the following order for coating film: LSGM>SDC>YSZ. The maximum power density of 197 and 100 mW/cm^2 can be achieved at 873 and 773 K, respectively, when LSGM film deposited on the anode side of LSGFM. Therefore, LSGFM can be used as electrolyte of SOFC operating at intermediate temperature.

In 2007, Polini, et al. [24] prepared $La_{0.8}Sr_{0.2}Ga_{0.8}Mg_{0.2-x}Co_xO_{3-\delta}$ (LSGMC) powders containing different amounts of Co ($x = 0.05$ and 0.085) by a citrate sol–gel method. The powders were used to prepare highly phase-pure LSGMC sintered pellets with controlled composition and fractional densities larger than 95%. For the first time, LSGMC materials were subjected to X-ray photoelectron spectroscopy (XPS) characterization. XPS data confirmed the presence of the dopants in the material and allowed to identify two different chemical states for Sr^{2+} and oxygen, both related to the oxygendeficient perovskite

structure of LSGMC. The conductivity of LSGMC sintered pellets containing different amounts of Co ions in the B sites of the perovskite lattice was assessed by electrochemical impedance spectroscopy (EIS) in the 250–750°C temperature range. Conductivity values and apparent activation energies were in good agreement with previously published data [30] referring to materials with same composition, but prepared by solid-state route. Therefore, the physicochemical and electrochemical characterization clearly demonstrated the ability of sol–gel methods to produce high-purity Co-doped LSGM perovskites, which represent promising solid electrolytes for intermediate-temperature SOFCs.

In 2005, Wang, et al. [25] investigated preparation, thermal expansion, electrical conductivity and polarization of $A_{2-\alpha}A'_{\alpha}BO_{4-\delta}$ type oxides (A=Pr, Sm, A'=Sr, B=Fe, Co) to evaluate their potential as cathode materials for IT-SOFCs. Within $0.8 \leq \alpha \leq 1.5$, $A_{2-\alpha}Sr_{\alpha}BO_{4-\delta}$ (A=Pr, Sm, B=Fe, Co) could be obtained as a single K_2NiF_4-structural phase. Thermal expansion coefficients (TECs) of the specimens increase with increasing Sr^{2+} content, TECs of cobaltites are much higher than that of ferrites. The electrical conductivity of cobaltites is in the order of 102 S cm^{-1} near 800 °C, which is acceptable for the cathode of IT-SOFC. Polarization measurements showed that $Sm_{0.5}Sr_{1.5}CoO_{4-\delta}$ exhibited the lowest cathodic overpotential at 700–900°C (72 mV at 500 mA/cm^2 at 800 °C), being a high potential candidate of cathode material for IT-SOFCs.

In 2006, Huang, et al. [26] synthesized $La_2NiO_{4+\delta}$ with a pure K_2NiF_4 by a polyaminocarboxylate complex precursor with diethylenetriaminepentaacetic acid (H_5DTPA) as ligand, and the electrical conducting properties of sintered $La_2NiO_{4+\delta}$ were investigated. The thermal decomposition of the complex precursor was investigated by thermogravimetry (TG) and differential scanning calorimetry (DSC). Homogeneous and fine powder (100–200 nm) with a pure K_2NiF_4 phase was produced by calcining the complex precursor at 900 °C for 2 h in air. It was found that $La_2NiO_{4+\delta}$ ceramic sintered at 1300 °C for 4 h shows a dense microstructure with average grain size of about 1 μm. The $La_2NiO_{4+\delta}$ ceramic exhibits an electrical conductivity of 76 Ω^{-1} cm^{-1} at 800°C. This research demonstrates the advantage of the polyaminocarboxylate complex method in preparing $La_2NiO_{4+\delta}$ with respect to the simplicity of synthesis process, fine and uniform morphology of synthesized powder and superior electrical conducting properties of sintered specimen.

In 2007, Dai, et al. [43] prepared $La_{1-x}Sr_xMO_{3-\delta}$ (M = Co, Mn; x = 0, 0.4) by coupling the methods of citric acid complexing and hydrothermal synthesis. The XRD results indicate that all the samples possessed single-phase rhombohedral crystal structures. The surface areas of these nanomaterials ranged from 20 to 33 m^2 g^{-1}, the achievement of such high surface areas are due to the uniform morphology with the typical particle size of 40–80 nm.

From many researches, it was shown that nanoscale perovskites enhance their physical and mechanical properties such as dielectric, ferroelectric, and conductivity etc. In addition, solvents and chelating agents used in the synthesis also play a critical role in determining the particle size of perovskite powder. Thus, in this research was attempt to reducing particle sizes by using various chelating agents and appropriate method. However, perovskite oxides were chosen by their property which proper for used as material in SOFC. Moreover, $Ba_{0.5}Sr_{0.5}Co_{0.8}Fe_{0.2}O_{3-\delta}$, $PrSrCoO_4$ and $PrSrNiO_4$ were used as cathode material. In addition, $La_{0.7}Sr_{0.3}Ga_{0.7}Fe_{0.2}Mg_{0.1}O_{3-\delta}$ and $La_{0.8}Sr_{0.2}Ga_{0.8}Mg_{0.15}Co_{0.05}O_{3-\delta}$ were used as electrolyte material in SOFC.

1.6 The objectives of the thesis

The objectives of this study are as follows:

1. To develop preparation method for reduction particle sizes of the following compounds
   - $Ba_{0.5}Sr_{0.5}Co_{0.8}Fe_{0.2}O_{3-\delta}$
   - $La_{0.7}Sr_{0.3}Ga_{0.7}Fe_{0.2}Mg_{0.1}O_{3-\delta}$
   - $La_{0.8}Sr_{0.2}Ga_{0.8}Mg_{0.15}Co_{0.05}O_{3-\delta}$
   - $PrSrCoO_4$
   - $PrSrNiO_4$

2. To study the properties of synthesized perovskite oxides for application in SOFC.